Journal of Power Sources 271 (2014) 16–24

Contents lists available at ScienceDirect

Journal of Power Sources

journal homepage: www.elsevier.com/locate/jpowsour

Improvement of oxygen diffusion characteristic in gas diffusion layer with planar-distributed wettability for polymer electrolyte fuel cell

Ryo Koresawa [a], Yoshio Utaka [b, *]

[a] Graduate School of Engineering, Yokohama National University, 79-5 Tokiwadai, Hodogaya, Yokohama 240-8501, Japan
[b] Faculty of Engineering, Yokohama National University, 79-5 Tokiwadai, Hodogaya, Yokohama 240-8501, Japan

HIGHLIGHTS

- A novel gas diffusion layer (hybrid GDL) was proposed for moisture control in PEFC.
- The hybrid GDL has alternate arrangement of regions of hydrophobic and hydrophilic.
- The hybrid GDL showed better effective oxygen diffusivity than usual GDL.
- The X-ray CT images showed variation of liquid water distribution in the GDL.
- The hybrid GDL with 10–20 mass% PTFE content has the highest oxygen diffusivity.

ARTICLE INFO

Article history:
Received 11 March 2014
Received in revised form
30 April 2014
Accepted 23 May 2014
Available online 2 August 2014

Keywords:
Polymer electrolyte fuel cell
Gas diffusion layer
Wettability distribution
X-ray computed tomography
Oxygen diffusivity
Galvanic cell oxygen absorber

ABSTRACT

Mass transfer characteristics of gas diffusion layer (GDL) are closely related to performance of polymer electrolyte fuel cells. Therefore, it is necessary to clarify the characteristics of water distribution relating to the microscopic conformation and oxygen diffusivity of GDL. A hybrid type carbon paper GDL with planar-distributed wettability is investigated for control of liquid water movement and distribution due to hydrophobic to hydrophilic areas that provide wettability differences in GDL and to achieve enhancement of both oxygen diffusion and moisture retention. Hybrid GDLs with different PTFE content were fabricated in an attempt to improve the oxygen diffusion characteristics. The effects of different PTFE contents on the oxygen diffusivity and water distribution were simultaneously measured and observed using galvanic cell oxygen absorber and X-ray radiography. The PTFE distribution was observed using scanning electron microscopy. The formation of oxygen diffusion paths was confirmed by X-ray radiography, where voids in the hybrid GDL were first formed in the hydrophobic regions and then spread to the untreated wetting region. Thus, the formation of oxygen diffusion paths enhanced the oxygen diffusion. In addition, the effects of local PTFE content in the hydrophobic region and the optimal amount of PTFE for hybrid GDL were elucidated.

1. Introduction and summary of former relevant studies

Polymer electrolyte fuel cells (PEFCs) are expected to be used as lightweight and reduced-size power sources for vehicles with low emission, due to their high power densities and superior start-up characteristics at low operating temperatures. Although PEFCs have become commercially available, many issues remain for further improvement of PEFC performance and to popularize PEFCs. Performance degradation by excess moisture in PEFCs is an especially important problem. For example, the diffusion of reactant gas is hindered at high humidity and high current density, because water or condensate from the humidified gas accumulates in the gas diffusion layer (GDL) and gas channels in the separator, which causes a decrease in the cell voltage. In contrast, proton conductivity in the polymer electrolyte is decreased by drying of the cell due to low humidity, which also decreases cell voltage. It is thus important to manage the amount of moisture at the cathode, where water is generated, due to the chemical reaction of hydrogen and oxygen. Therefore, the liquid water distribution and mass transfer characteristics of the reactant gas in the cathode GDL, where the generated vapor condenses, must be clarified. Apart from the liquid water distribution, it is also necessary to characterize the microscopic conformation and oxygen diffusivity of a GDL containing moisture.

* Corresponding author. Tel./fax: +81 45 339 3909.
E-mail address: utaka@ynu.ac.jp (Y. Utaka).

http://dx.doi.org/10.1016/j.jpowsour.2014.05.151
0378-7753/

The characteristics of liquid water and oxygen diffusion in the GDL of microporous media of PEFC have been previously investigated. Techniques such as fluorescence microscopy [1,2], neutron radiography [3,4] and X-ray radiography [5–14] have been used to visualize and analyze the microscopic configuration and distribution of liquid water in PEFCs and GDLs. Sasabe and colleagues [7–9] visualized and analyzed the liquid water behavior inside PEFC under power generation using soft X-rays. Moreover, analyses using synchrotron X-rays with high flux have been performed [10–14]. The internal conformation and liquid water distribution in arbitrary sections of PEFCs under power generation were visualized using X-ray computer tomography (CT) by Krüger et al. [13,14]. Other than the visualizations of GDLs, hydrophobic treatment and microporous layer (MPL) coating of GDLs were investigated to improve the PEFC performance. Thus, the effects of hydrophobic polymer quantity in a GDL [15–21] and a GDL with MPL [21–25] on PEFC performance have been examined. Hydrophobic treatment of GDLs was investigated using polytetrafluoroethylene (PTFE) [15–19] or fluorinated ethylene propylene (FEP) [20,21]. Other than the water management in a GDL by application of hydrophobic treatment and MPL coating, the effect of GDLs with holes or slit has also been attempted [26–29]. To enhance liquid water transport from the GDL to the gas channels and to realize lower mass transport losses of oxygen through the GDL, systematic modification of the GDL with laser-treated 39 holes (approximately 80 μm diameter) along the center of the gas channel, has been conducted using laser-perforation by Gerteisen et al. [26]. Manahan et al. [27] prepared a laser-treated GDL with MPL that had holes (ca. 300 μm diameter) formed at regular intervals, and the performance for liquid water transport was enhanced. Kimball et al. [28] attempted to control the liquid water behavior by creating a large single diameter pore in the GDL under a rib or channel. To promote the discharge of condensate water that stagnates in the GDL, a slit was created in the GDL and the fuel cell performance was investigated by Nishida et al. [29].

A method has been developed to measure the effective oxygen diffusivity in porous media using a galvanic cell oxygen absorber [30], and a method to measure the effective oxygen diffusivity of GDL containing moisture [31] has been proposed by the authors. In addition, the measurement accuracy of the oxygen diffusion characteristics in a GDL was enhanced by improvement of the oxygen absorber and verification of the measurement method [32]. Furthermore, the liquid water distribution and behavior in porous media have also been visualized using neutron radiography [33,34], where simultaneous measurement of the liquid water behavior and oxygen diffusion characteristics in GDLs was conducted. Novel GDL configurations have been proposed (hybrid type GDL) to improve the oxygen diffusivity by controlling the moisture distribution and movement in the GDL, in which two porous media with different wettabilities [35] or pore size distributions [36] are arranged alternately. Liquid water distributions were visualized and the oxygen diffusion characteristics were measured [35]. The concept of the hybrid GDL was applied using a carbon paper GDL treated with PTFE. A carbon paper GDL with non-uniform wettability distribution was prepared by forming alternately arranged adjacent regions of hydrophobic (with PTFE) and hydrophilic areas [37]. The hybrid GDL has much higher oxygen diffusivity than conventional GDLs by control of the liquid water movement from hydrophilic to hydrophobic regions. Moreover, the effects of average PTFE concentrations on the oxygen diffusion characteristics were examined by changing the hydrophobic PTFE content in the hybrid GDL [38].

The objective of this study is to further elucidate the effects of the liquid water distribution in the hybrid GDL on the oxygen diffusion characteristics by extensively changing the PTFE content in the hydrophobic region of the hybrid GDL. Therefore, hybrid GDLs with different forms of hydrophobic regions and various PTFE contents were fabricated, and local PTFE content of the hydrophobic region in the hybrid GDL was analyzed in detail. Elucidation of the relationship between the variations of liquid water distribution and the oxygen diffusion characteristics in the GDL was attempted by simultaneous measurement of the oxygen diffusivity and the liquid water distribution. The oxygen diffusivity was measured using a galvanic cell oxygen absorber and the characteristics of liquid water distributions were quantitatively evaluated using X-ray CT at the SPring-8 synchrotron radiation facility. Furthermore, the local PTFE content of the hydrophobic region was evaluated by surface observation of the hybrid GDL using electron microscopy. Based on this evaluation and the oxygen diffusivity measurement using the oxygen absorber apparatus, the effects of PTFE content on the oxygen diffusion characteristics and optimal amount of PTFE for the hybrid GDL were investigated in an attempt to enhance the oxygen diffusivity. Although the drying process of a GDL was adopted for varying the water saturation in this study, in which the rate and method of water supply is different from those in actual PEFC, it is significant to elucidate the relationship between the water movement phenomena and the oxygen diffusion characteristics in the GDL.

2. Experimental setup and procedure

2.1. Galvanic cell oxygen absorber apparatus for diffusivity measurement and determination of effective diffusivity

The galvanic cell oxygen absorber apparatus for measurement of the oxygen diffusion characteristics in the GDL is shown in Fig. 1. The fundamental structure of the galvanic cell oxygen absorber was basically the same as that presented in our previous report [32]; however, some improvements were made to visualize the interior of the GDL using X-rays. X-ray visualization was enabled by altering the position of the GDL from the oxygen absorbing surface from 3.1 mm to 13.6 mm to locate the GDL sample between the X-ray source and detector. The galvanic cell oxygen absorber consists of a carbon electrode film (cathode), a lead electrode plate (anode), and an electrolyte of principally potassium hydroxide solution. The hydrophobic carbon film cathode acts as an oxygen penetration diaphragm that separates the atmosphere and electrolyte, but allows oxygen in the atmosphere to penetrate and undergo electrochemical reaction. According to the electrochemical reaction for Galvanic battery, which was elucidated by Clark et al. [39], the electrochemical reactions at the two electrodes are expressed as:

$$\left[\text{Cathode}\right] \quad O_2 + 2H_2O + 4e^- \rightarrow 4OH^- \tag{1}$$

$$\left[\text{Anode}\right] \quad 2Pb \rightarrow 2Pb^{2+} + 4e^- \tag{2}$$

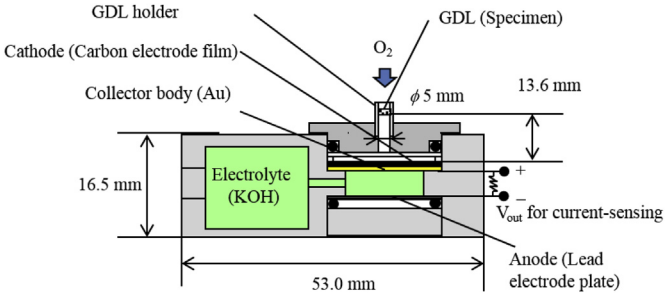

Fig. 1. Schematic diagram of galvanic cell oxygen absorber apparatus for oxygen diffusivity measurement for simultaneous measurement with X-ray imaging.

At the cathode, the reduction of oxygen occurs when oxygen penetrates the cathode and dissolves into the electrolyte. As a result, the experimental apparatus effectively functions as an oxygen absorber. Corresponding to this process, the lead anode is oxidized according to the chemical reaction given in Eq. (2). Lead dissolves in the alkaline electrolyte and water is produced in the same quantity as the amount consumed at the cathode, according to:

$$Pb^{2+} + 3OH^- \rightarrow HPbO_2^- + H_2O \quad (3)$$

The quantity of oxygen gas consumed by the electrochemical reaction at the cathode can be obtained from the output current I [A] of the oxygen absorber using Eq. (4). Thus, the output current resulting from oxygen reduction due to reaction at the cathode surface is determined by measuring the voltage drop across an in-circuit resistor from the electromotive force of the oxygen absorber.

$$J_{O_2} = 31.99 \times 10^{-3} \times \frac{I}{4F} \times \frac{1}{A} \quad (4)$$

where J_{O_2} kg (m^{-2} s^{-1}), F (s·A)/mol and A (m^2) are the oxygen mass flux, the Faraday constant and the cross-sectional area of the carbon electrode film, respectively. The four electrons chemical reaction shown in Eqs. (1) and (2) was confirmed experimentally by Utaka et al. [30]. As described in [31], the comparison method has developed to determine the effective oxygen diffusivity of GDL, where the mass transfer conductance of a standard test sample with a known diffusion coefficient is measured consecutively under the same experimental conditions for the test the sample measurement. The effective oxygen diffusion coefficient for the test sample was determined by adopting the bulk characteristics of oxygen reaction in the galvanic cell oxygen absorber as a variation of the effective diffusion resistance. Since the apparatus configuration along the direction of the oxygen path is two-dimensionally axisymmetric as shown in Fig. 1, the distribution and oxygen flux were calculated numerically to determine the effective oxygen diffusivity.

The GDL sample was inserted into a cylindrical acrylic pipe (0.5 mm thick, 5 mm inner diameter). The sample was installed over the oxygen absorbing surface to permit simultaneous measurement of the oxygen diffusivity and visualization of liquid water in the GDL by X-ray CT. A thin cylindrical acrylic pipe was used in consideration of the X-ray transmission. One side of the installed GDL sample containing moisture was exposed to the atmosphere, as shown in Fig. 1, at the start of the oxygen diffusivity measurement. The oxygen diffusivity measurement was performed during the drying process of a wet GDL.

2.2. X-ray CT imaging for observation of liquid water distribution in GDL

A high speed and high resolution visualization technique was required to evaluate the liquid water distribution in the GDL, which consists of carbon fiber (ca. 8 μm diameter), to simultaneously measure the oxygen diffusion characteristics. X-ray CT was conducted at the BL20B2 beam line of SPring-8 [40] as a non-destructive technique to obtain 3D internal structural information of the sample by measuring the spatial distribution of the X-ray attenuation coefficient and reconstructing the data. CT images were acquired within a short time using monochromatic X-ray with high luminance and high directivity (ca. 1 min/measurement). Moreover, it is possible to use an imaging process that utilizes X-ray refraction, which is effective for small samples that have different attenuation coefficients. Fig. 2 shows a schematic of the projection tomographic X-ray system with the BL20B2 beam line. X-rays passing through the object are transformed into a visible image by the fluorescent screen (scintillator). The visible light images on the screen are projected by an optical lens system and are detected by a complementary metal oxide semiconductor (CMOS) image sensor. Table 1 lists the projection imaging conditions used for the BL20B2 beam line.

2.3. GDL test samples

Carbon paper (Toray, TGP-H-120) with a thickness of 370 μm was used as a GDL sample. The method of PTFE treatment is as follows. PTFE powders (particle size: 0.15–0.35 μm) were dispersed in water and stabilized with a non-ionic surfactant and flowed into the GDL carbon paper together with air using vacuum suction. PTFE particles remain and adhere inside the GDL. The PTFE particles are then melted and fixed to the carbon fiber in the GDL by heating. Hybrid GDLs with partial hydrophobic regions were prepared [37]. Detailed specifications of the GDLs that were prepared for simultaneous oxygen diffusivity measurement and X-ray visualization are given in Table 2. Details of the GDLs that were used for oxygen diffusivity measurements and the scanning electron microscopy (SEM; Keyence, VE-8800) surface observation are given in Table 3. Two types of hybrid GDLs with different hydrophobic regions (dot and stripe) were prepared. Fig. 3 shows schematic diagrams and typical CT images of the untreated GDL and hybrid GDLs. The CT images show hybrid GDLs with 41 and 43 mass% PTFE content (the PTFE content denotes the locally averaged PTFE content at the hydrophobic region). The carbon paper GDL entries in Tables 2 and 3 and Fig. 3 indicate non-treated and uniformly-treated carbon paper. The local PTFE content of the hybrid GDL denotes the ratio of mass of PTFE to that in the original non-treated GDL in the hydrophobic region. The dotted lines in Fig. 3 show the boundaries between the hydrophobic region and the untreated region, which is referred to as the hydrophilic region. Furthermore, the volumes of the hydrophobic and hydrophilic regions were almost equivalent. In the stripe hybrid GDL, the width of the hydrophobic region was approximately 1.5–2.0 mm. In the dot hybrid GDL, the radius of the hydrophobic region was approximately 1.0–1.5 mm. The CT images in Fig. 3 show the GDLs within the cylindrical acrylic pipe (gray circular area surrounding the GDL) with three different shades of darkness in the dry GDL; the darkest, middle and light colored areas denote pores (air), carbon fibers, and PTFE, respectively. In the wet GDL, the gray color denotes the area filled with liquid water among carbon fibers. The area of hydrophobic region denotes the ratio of the hydrophobic region to the total volume. The hybrid GDLs were classified into 5 categories according to the PTFE content: approximately 10 (7–14 mass%), 20 (15–24 mass%), 30 (26–33 mass%), 40 (41–43 mass%) and 50 (45–52 mass%). Although the measured values are in parentheses, the representative numbers were used for simple expression. The average porosity of the hybrid GDL was calculated from the additional mass of PTFE. The evacuation impregnation method [31] was used to fill the GDLs with water.

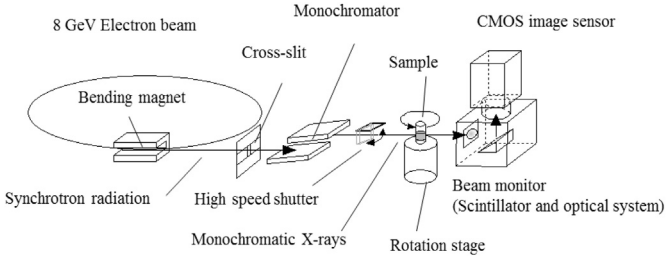

Fig. 2. Outline of projection tomographic X-ray system.

Table 1
Projection imaging conditions of the BL20B2 beam line.

Photon energy [keV]	13
Effective pixel size [μm/pixel]	3.94
Distance between sample and detector [mm]	55
Exposure time [ms]	70
Number of projection [/180°]	1500/180

Table 2
Specifications for GDLs (Simultaneous oxygen diffusivity measurement and visualization).

GDL type	Local PTFE content/mass%	Area of hydrophobic region/%	Porosity	Thickness/μm
Carbon paper GDL	–	–	0.78	370
(uniform)	6	100	0.76	
	23	100	0.72	
Dot hybrid GDL	8	50	0.76	
	14	46	0.75	
	16	41		
	24	54	0.73	
	43	59	0.70	
Stripe hybrid GDL	7	54	0.76	
	15	45	0.75	
	18	57	0.74	
	31	54	0.72	
	43	42		
	41	51	0.71	
	43	46		
	46	55	0.70	

Table 3
Specifications for GDLs (Oxygen diffusivity measurement and SEM observation).

GDL type	Local PTFE content/mass%	Area of hydrophobic region/%	Porosity	Thickness/μm
Carbon paper GDL	–	–	0.78	370
(uniform)	6	100	0.76	
	23	100	0.72	
	33	100	0.68	
Dot hybrid GDL	18	42	0.75	
	16	52		
	24	30		
	22	45	0.74	
	31	36		
	33	34		
	26	52	0.73	
	27	47		
		55		
	31	45		
	45	34	0.72	
	47	37	0.71	
	52	29		
Stripe hybrid GDL	16	52	0.75	
	21	47	0.74	
	30	43	0.73	
	32	43		
	32	46		
	46	38	0.72	
	45	39	0.71	
	48	33		
	45	41		

3. Results and discussion

3.1. Effect of PTFE treatment on porosity of hydrophobic GDL

The porosity distributions of three untreated GDL samples with uniform wettability distributions calculated from the image data processing are shown in Fig. 4. Fig. 5 shows typical CT images of an untreated GDL (GDL1 shown in Fig. 4). The average porosity is calculated from the cross-sectional image (y-z plane) within the solid line and at the position shown by the dashed line in Fig. 5(a) and (b). The porosity distribution is obtained from binarized CT images of the GDLs. GDL1, 2, 3 in Fig. 4 are made from the same type of carbon paper (TGP-H-120), and the porosity distributions are measured at different positions in the cross-sectional images. The average porosity of each GDL is 0.78. Although the local porosity is distributed, the average porosity for the entire region of each GDL is almost the same.

Fig. 6(a) and (b) show the porosity distribution and data processing area of a stripe hybrid GDL that contains 41 mass% PTFE, respectively. Fig. 6(a) shows the average porosities at the y-z section in Fig. 6(b) and that of the untreated GDLs shown in Fig. 5. The regions surrounded with the dashed line in Fig. 6(a) and (b) are the hydrophobic areas treated with PTFE. The average porosity over the entire region of the hybrid GDL is 0.71 and the hydrophobic region has lower porosity than the average. The positions of the hydrophobic regions shown in Fig. 6(a) and (b) correspond well with each other. The volumetric fraction of hydrophobic region is about 51% with the PTFE content of 41 mass% in the hydrophobic region; therefore, the overall average porosity was decreased by PTFE treatment. As shown in Section 3.3, the oxygen diffusivity in the dry hybrid GDL decreases due to the decrease in porosity.

3.2. Determination of PTFE content in hydrophobic region by the SEM surface observation of hybrid GDLs

Fig. 7 shows SEM micrographs of the obverse and the reverse sides of the hybrid GDL. The central light colored regions indicated by the dashed lines is the hydrophobic region in which the pores among the carbon fibers are partially occupied by PTFE. The hydrophobic region in Fig. 7(b) occupies a wider fraction than that shown in Fig. 7(a), because the PTFE dispersion liquid flows into the reverse side from the obverse side with lateral diffusion due to wetting of the carbon fibers during the PTFE treatment process. The hydrophobic region in the hybrid GDL is calculated using the average area of both surfaces of the GDL.

3.3. Simultaneous measurement of oxygen diffusivity and visualization of liquid water distribution

Fig. 8 shows the results of the simultaneous measurement of the oxygen diffusivity and visualization of the liquid water distribution for the untreated carbon paper GDL with uniform wettability distribution. The relation between the effective oxygen diffusivity of the GDL and the average water saturation, which denotes the fraction of pores filled with water (all pores are filled with water at 100% saturation), is given. The average saturation of the GDL is determined by binarizing the CT images (approximately 100 images/plot) of the GDL with reference to the dry GDL images, i.e., the threshold is used to calculate the saturation from the images by comparison with the porosity of the dry GDL. Fig. 8 shows the variation of liquid water distribution in the CT images of the GDL with the change in saturation during the drying process from the surface, which is correlated with the oxygen diffusivity. These images show only the liquid water (light color), because the CT image for the dry GDL is subtracted from the CT images of the GDL containing moisture. Thus, dark areas in Fig. 8 indicate the regions without liquid water. The CT images are cross-sectional images perpendicular to the thickness direction. The oxygen diffusivity in the carbon paper GDL increases with decreasing water saturation, due to an increase in oxygen diffusion paths along vacant pores. The oxygen diffusivity results are in good agreement with the previous

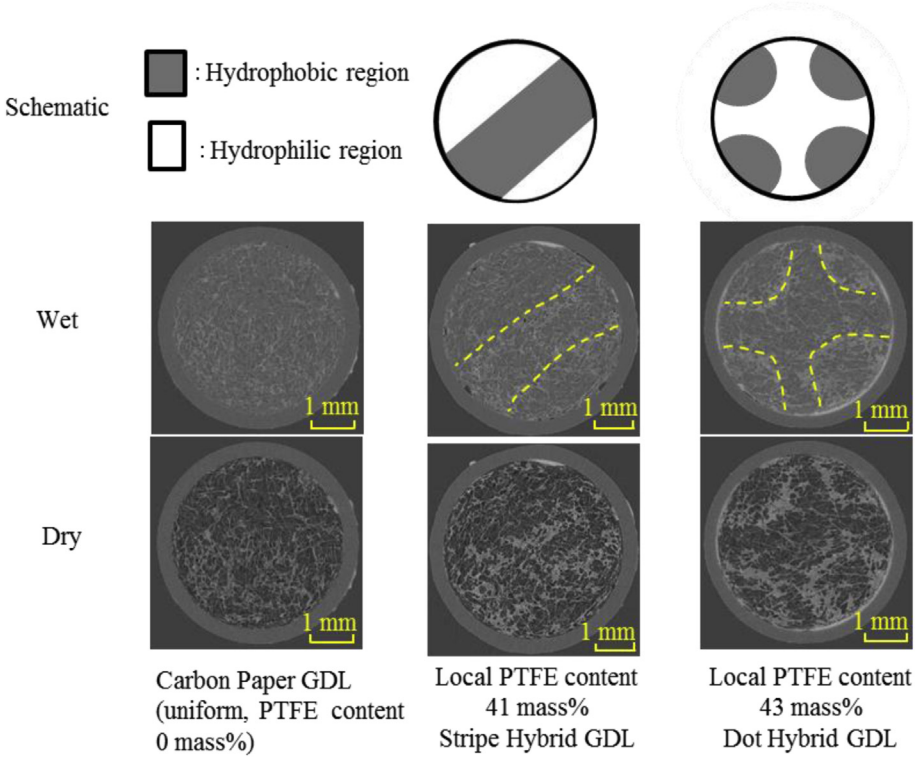

Fig. 3. Schematic diagrams and X-ray CT images of the GDLs.

report, which confirms that such measurements using the improved oxygen absorber for X-ray visualization are performed with sufficiently high precision. The CT visualization images reveal that the oxygen diffusion paths (pores in the GDL) are formed increasingly with increasing oxygen diffusivity. While the CT images imply that initial pores are formed at irregular sites, the pores spread from the initial pores to the entire GDL.

Fig. 9 shows the results of simultaneous measurement of the oxygen diffusivity and visualization of liquid water distribution for a stripe hybrid GDL (striped hydrophobic region with 41 mass% PTFE). The gray area in the schematic diagram at the top-left of Fig. 9 indicates the hydrophobic region of the hybrid GDL. The oxygen diffusivity in both the carbon paper GDL and the hybrid GDL increases with decreasing average water saturation, because the oxygen diffusion paths increase due to an increase of pores. The difference in the oxygen diffusivity of these two types of GDLs is more prominent with decreasing average water saturation at approximately 60% or less. The hybrid GDL with non-uniform wettability distribution exhibits high oxygen diffusion characteristics. For example, at an average water saturation of approximately 20%, the oxygen diffusivity in the hybrid GDL is approximately 2.5–3 times higher than that in the untreated carbon paper GDL. The variation of the liquid water distribution and formation of pores evident in the CT images of the hybrid GDL indicates the

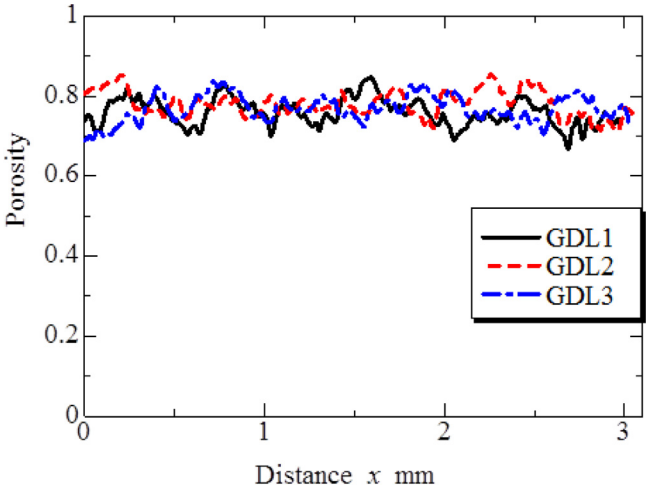

Fig. 4. Porosity distribution of untreated carbon paper GDL with 0 mass% PTFE content.

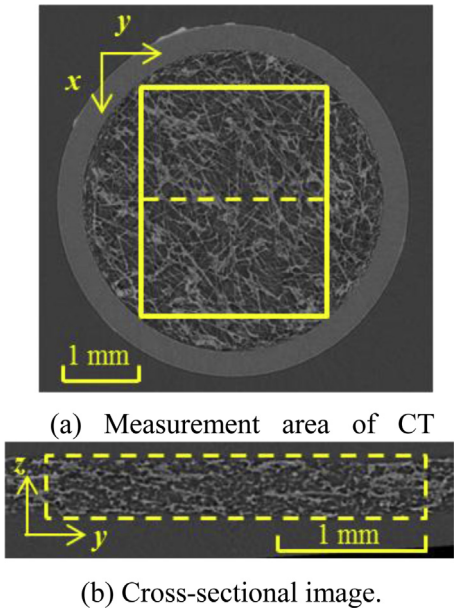

Fig. 5. Measurement area of untreated carbon paper GDL with 0 mass% PTFE content.

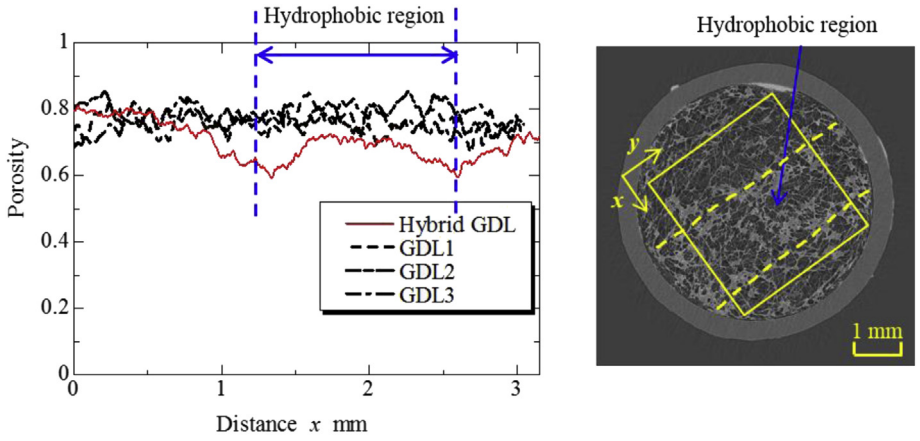

(a) Porosity distribution. (b) Measurement area

Fig. 6. Porosity distribution and measurement area.

variation of oxygen diffusivity. After the pores in the hybrid GDL are formed in the hydrophobic region near the wettability boundary, the pores are enlarged to the hydrophilic region. The main reason for the formation of pores and enhancement of the effective oxygen diffusivity is the movement of liquid water by liquid drawing of the hydrophilic region from the hydrophobic region, as previously reported in Refs. [37] and [38]. Therefore, it is considered that pores are formed at the wettability boundary with the hydrophobic region by liquid water movement from the hydrophobic region to the hydrophilic region, and that oxygen diffusion paths are formed continuously in the thickness direction of the GDL independently of the moisture change mechanism. Thus, the formation of oxygen diffusion paths enhances oxygen diffusion. Moreover, there is no difference in the evaporation rates for both the non-wettable GDL (uniform wettability distribution) and wettable GDL (uniform wettability distribution) [35], which confirms that the oxygen diffusivity is not enhanced by a difference in the evaporation rate, but by the movement of liquid water from the hydrophobic region to the hydrophilic region. Very slowly changes of water saturations as measurement times of about 1200 and 1800s for the cases shown in Figs. 8 and 9, respectively, were given in this study.

Figs. 10 and 11 show the variations in the liquid water distributions of the GDLs with cross-sectional CT images of the carbon paper GDL with uniform wettability and a hybrid GDL with a non-uniform wettability distribution (41 mass% stripe hybrid GDL), respectively, which correspond to Figs. 8 and 9, respectively. Liquid water is indicated by light gray color and the black areas indicate no water. The oxygen diffusion paths increase gradually by the evaporation of liquid water from the top surface for the untreated uniform wettability GDL. These cross-sectional images imply that pores are formed irregularly in the untreated carbon paper GDL with decreasing water saturation. Fig. 11 shows the reduction of liquid water in the hybrid GDL starts predominantly from hydrophobic region. Fig. 11(e) represents the dry condition and Fig. 11(b)–(d) indicates the conditions with liquid water present mainly in the hydrophilic region and with oxygen diffusion paths formed at the hydrophobic regions. It is considered that the hybrid GDL has much higher oxygen diffusivity than the carbon paper GDL with uniform wettability distribution, due to the oxygen diffusion paths formed continuously in the thickness direction. Since the water saturation varies with time very slowly by giving drying process in this experiment, there is not exact correspondence between the conditions of water generation in between this experiment and the actual operation of PEFC. Therefore, it is necessary further to investigate the effect of rate of liquid water movement considering the water generation under the actual condition.

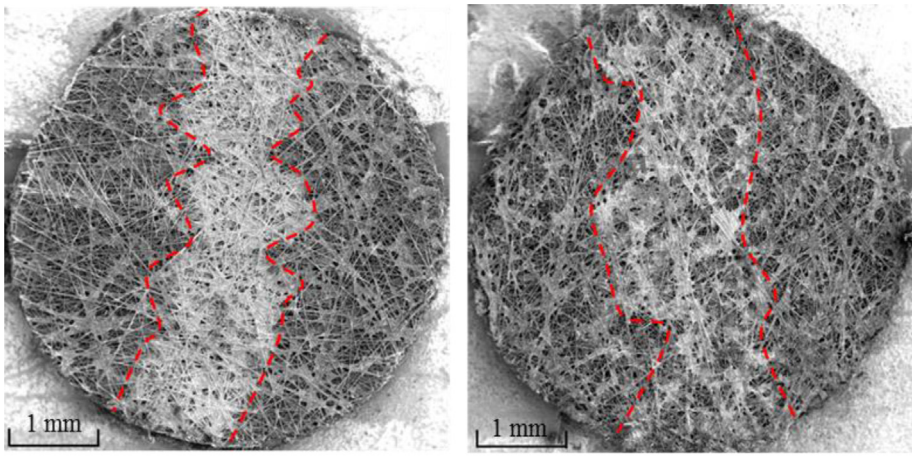

(a) Obverse side of hybrid GDL (b) Reverse side of hybrid GDL

Fig. 7. SEM micrographs of the surface morphology of the hybrid GDL.

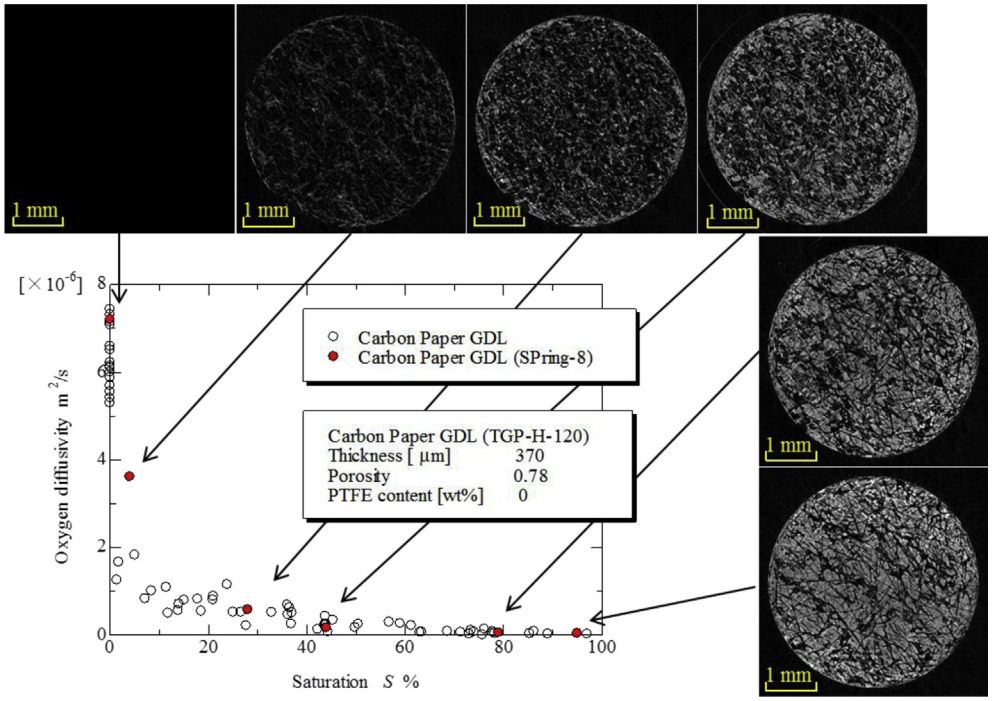

Fig. 8. Oxygen diffusivity as a function of the average saturation in untreated carbon paper GDL with 0 mass% PTFE content with corresponding CT images.

3.4. Oxygen diffusion characteristics in GDLs with/without wettability distribution and the effect of PTFE content in the hydrophobic region

Fig. 12 shows the effective oxygen diffusivities for the non-treated GDLs, the uniformly-treated GDLs and the hybrid GDLs with various PTFE content. Specifications for these GDLs are shown in Tables 2 and 3 The hybrid GDLs are classified into five categories according to the PTFE content (approximately 10, 20, 30, 40 and 50 mass%), as described in Section 2.3. Also, PTFE mass% of uniformly-treated GDLs correspond to PTFE mass% of the hybrid GDLs. The average saturation in the measurement of oxygen diffusivity is calculated from mass measurements. The oxygen diffusivity increases when the water saturation decreases from 100%. Significant differences in the oxygen diffusivity appear when the average water saturation is 60% or less. The oxygen diffusivities

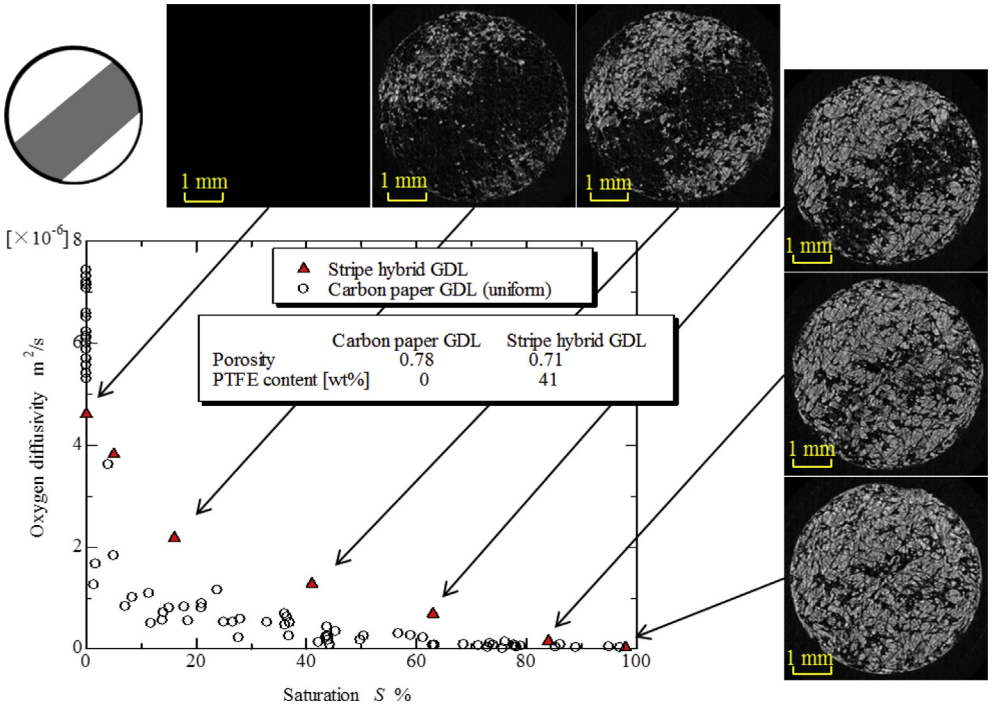

Fig. 9. Oxygen diffusivity in stripe hybrid GDL with non-uniform wettability distribution as a function of the average saturation with corresponding CT images.

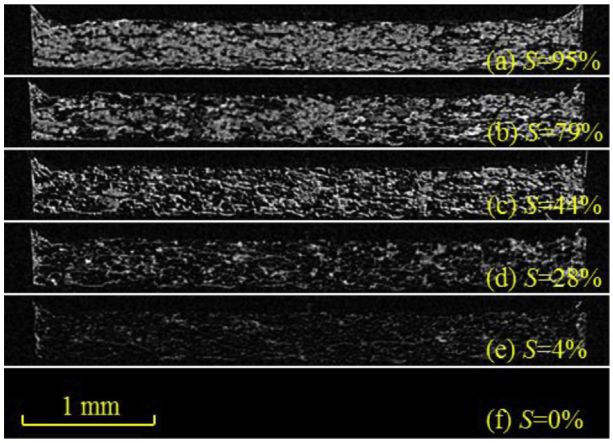

Fig. 10. Cross-sectional images of the untreated carbon paper GDL with 0 mass% PTFE content.

in the hybrid GDLs are higher than that in the untreated carbon paper GDL without wettability distribution. Furthermore, in comparison of the oxygen diffusivities with PTFE uniformly-treated GDLs and the hybrid GDLs, both GDLs show similar characteristics of the oxygen diffusion at the low range of water saturation. In contrast, at the relatively higher range of water saturation (approximately from 30 to 60%), which is considered to correspond to the high current density region in the power generation, the oxygen diffusivities in the hybrid GDLs are higher than that in PTFE uniformly-treated GDLs. Those results show the similar tendency of author's previous result [35], which was conducted by two porous media with different wettability simulating hybrid GDL. Therefore, in the real power generation, it is probable that the hybrid GDL are especially effective in case of relatively high current density, in which liquid water is generated readily. Comparison of the oxygen diffusivity in the hybrid GDLs with various PTFE content reveals corresponding differences. The hybrid GDL with approximately 20 mass% PTFE has the highest oxygen diffusivity, which is approximately three times that for the untreated carbon paper GDL in the range of average water saturation (ca. 5–60%). The oxygen

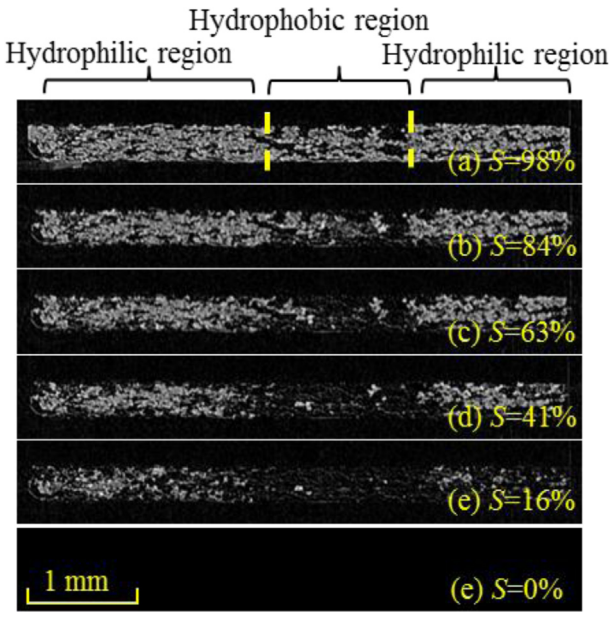

Fig. 11. Cross-sectional images of hybrid GDL with wettability distribution.

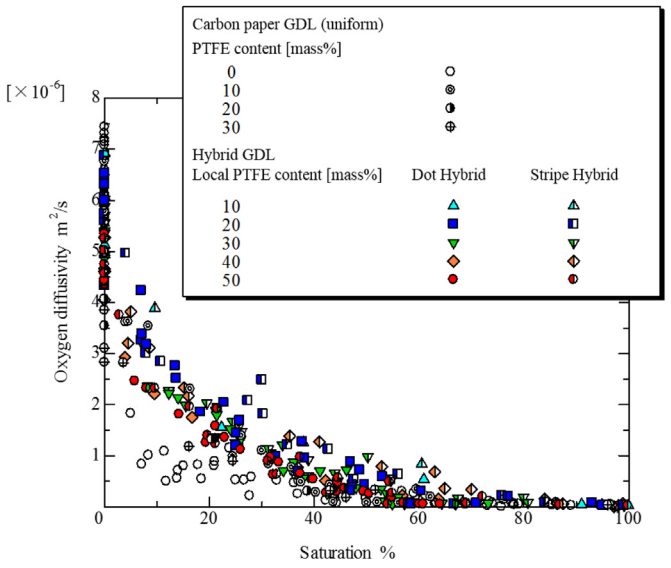

Fig. 12. Effective oxygen diffusivity as a function of the average saturation for various GDLs.

diffusivity in the hybrid GDLs with 50 mass% PTFE is the lowest of the hybrid GDLs. The oxygen diffusivity in the hybrid GDLs with approximately 10–20 mass% PTFE are comparable with that for the untreated carbon paper GDL when the average water saturation is 0% (dry condition), while those for GDLs with PTFE content ranging from approximately 30 to 50 mass% are lower, because PTFE occupies the pores and partially restricts oxygen diffusion. These results indicate that the optimal amount of PTFE for a hybrid GDL is from approximately 10 to 20 mass%.

Two types of hydrophobic region shape are prepared in hybrid GDLs (striped type and dotted type) to examine the effects of boundary length between the hydrophobic and hydrophilic regions on the oxygen diffusion characteristics. However, there is no significant difference between the oxygen diffusivity of the striped and dotted hydrophobic regions. In both cases, it is considered that the oxygen diffusion characteristics are dependent on the area of hydrophobic region because liquid water in hydrophobic region is mostly removed before that in the hydrophilic region under the present experimental conditions. In our previous report using simulated test samples [35], the effect of the pitch of the hydrophilic and hydrophobic media is examined experimentally and the oxygen diffusivity is improved by decreasing the pitch (increasing the boundary length of the hydrophobic and hydrophilic media). Therefore, it is probable that the oxygen diffusion characteristics can possibly be further improved by decreasing the interval of arrangement.

4. Conclusions

The effective oxygen diffusivity characteristics of hybrid GDLs with non-uniform wettability distribution were investigated by simultaneous measurement of oxygen diffusivity and visualization of the liquid water in carbon paper type GDLs. The effects of the wettability distribution and PTFE content in the hydrophobic region of the GDLs on effective oxygen diffusivity were examined. The results are summarized as follows:

[1] The hydrophobic region of the hybrid GDL can be distinguished by visualization using X-ray CT and an SEM surface observation.

[2] In carbon paper type GDLs for PEFC with wettability distribution (hybrid GDL), oxygen diffusion paths were formed in the hydrophobic region near the boundary between the hydrophilic and hydrophobic regions, due to the drawing of water into the hydrophilic region so that the entire hydrophobic region was enlarged.
[3] The effective oxygen diffusivity in the hybrid GDL containing moisture is higher than that in the carbon paper GDL with uniform wettability distribution because oxygen diffusion is promoted by the formation of pores in the hydrophobic region.
[4] The hybrid GDL with approximately 10–20 mass% PTFE in the hydrophobic area has the highest effective oxygen diffusivity and is approximately three times higher than that in the carbon paper GDL with uniform wettability in the water saturation range of approximately 5–60%. However, the oxygen diffusivity in the hybrid GDLs with high PTFE content is low in the range of low water saturation, because the pores are partially filled by PTFE, which constricts oxygen diffusion paths.

Acknowledgments

This work was supported in part by a Grant-in-Aid for Scientific Research [23360097] from the Japan Society for the Promotion of Science (JSPS), the Strategic International Collaborative Research Program of the Japan Science and Technology Agency (JST). The synchrotron radiation experiments were performed at the BL20B2 beam line of SPring-8 as a Priority Research Proposal with the approval of the Japan Synchrotron Radiation Research Institute (JASRI) (Proposal Nos. 2011B1819, 2011B1825, 2012A1632 and 2012B1745).

References

[1] S. Litster, D. Sinton, N. Djilali, J. Power Sources 154 (2006) 95–105.
[2] A. Bazylak, D. Sinton, N. Djilali, J. Power Sources 176 (2008) 240–246.
[3] P. Boillat, D. Kramer, B.C. Seyfang, G. Frei, E. Lehmann, G.G. Scherer, A. Wokaun, Y. Ichikawa, Y. Tasaki, K. Shinohara, Electrochem. Commun. 10 (2008) 546–550.
[4] M. Weiland, P. Boillat, P. Oberholzer, A. Kaestner, E.H. Lehmann, T.J. Schmidt, G.G. Scherer, H. Reichl, Electrochim. Acta 87 (2013) 567–574.
[5] P.K. Sinha, P. Halleck, C.Y. Wang, Electrochem. Solid-state Lett. 9 (2006) A344–A348.
[6] W.K. Epiting, J. Gelb, S. Lister, Adv. Funct. Mater. 22 (2012) 555–560.
[7] T. Sasabe, S. Tsushima, S. Hirai, Int. J. Hydrogen Energy 35 (2010) 11119–11128.
[8] P. Deevanhxay, T. Sasabe, S. Tsushima, S. Hirai, Int. J. Hydrogen Energy 36 (2011) 10901–10907.
[9] P. Deevanhxay, T. Sasabe, S. Tsushima, S. Hirai, J. Power Sources 230 (2013) 38–43.
[10] C. Hartnig, I. Manke, R. Kuhn, S. Kleinau, J. Goebbels, J. Banhart, J. Power Sources 188 (2009) 468–474.
[11] S.J. Lee, S.G. Kim, G.G. Park, C.S. Kim, Int. J. Hydrogen Energy 35 (2010) 10457–10463.
[12] R. Flückiger, F. Marone, M. Stampanoni, A. Wokaun, F.N. Büchi, Electrochim. Acta 56 (2011) 2254–2262.
[13] P. Krüger, H. Markötter, J. Haussmann, M. Klages, T. Arlt, J. Banhart, C. Hartnig, I. Manke, J. Scholta, J. Power Sources 196 (2011) 5250–5255.
[14] H. Markötter, I. Manke, P. Krüger, T. Arlt, J. Haussmann, M. Klages, H. Riesemeier, C. Hartnig, J. Scholta, J. Banhart, Electrochem. Commun. 13 (2011) 1001–1004.
[15] D. Bevers, R. Rogers, M. Bradke, J. Power Sources 63 (1996) 193–201.
[16] J. Moreira, A.L. Ocampo, P.J. Sebastian, M.A. Smit, M.D. Salazar, P. Angel, J.A. Montoya, R. Perez, L. Martinez, Int. J. Hydrogen Energy 28 (2003) 625–627.
[17] G.G. Park, Y.J. Sohn, T.H. Yang, Y.G. Yoon, W.Y. Lee, C.S. Kim, J. Power Sources 131 (2004) 182–187.
[18] K.T. Cho, M.M. Mench, J. Power Sources 195 (2010) 6748–6757.
[19] R.J.F. Kumar, V. Radhakrishnan, P. Haridoss, Int. J. Hydrogen Energy 37 (2012) 10830–10835.
[20] C. Lim, C.Y. Wang, Electrochim. Acta 49 (2004) 4149–4156.
[21] W.M. Yan, C.Y. Hsueh, C.Y. Soong, F. Chen, C.H. Cheng, S.C. Mei, Int. J. Hydrogen Energy 32 (2007) 4452–4458.
[22] Z. Qi, A. Kaufman, J. Power Sources 109 (2002) 38–46.
[23] S. Park, J.W. Lee, B.N. Popov, J. Power Sources 163 (2006) 357–363.
[24] H.K. Atiyeh, K. Karan, B. Peppley, A. Phoenix, E. Halliop, J. Pharoah, J. Power Sources 170 (2007) 111–121.
[25] S. Park, J.W. Lee, B.N. Popov, J. Power Sources 177 (2008) 457–463.
[26] D. Gerteisen, T. Heilman, C. Ziegler, J. Power Sources 177 (2008) 348–354.
[27] M.P. Manahan, M.C. Hatzell, E.C. Kumbur, M.M. Mench, J. Power Sources 196 (2011) 5573–5582.
[28] E.E. Kimball, J.B. Benziger, Y.G. Kevrekidis, Fuel Cells 10 (2010) 530–544.
[29] K. Nishida, T. Murakami, S. Tsushima, S. Hirai, J. Power Sources 195 (2010) 3365–3373.
[30] Y. Utaka, Y. Tasaki, S. Wang, T. Ishiji, S. Uchikoshi, Int. J. Heat Mass Transf. 52 (2009) 3685–3692.
[31] Y. Utaka, D. Iwasaki, Y. Tasaki, S. Wang, Heat Trans. Res. 39 (2010) 262–276.
[32] R. Koresawa, T. Daitoku, Y. Utaka, Trans. JSME (B) 77 (2011) 2191–2199.
[33] Y. Utaka, Y. Tasaki, S. Wang, D. Iwasaki, N. Waki, N. Kubo, K. Shinohara, P. Boillat, G. Frei, P. Oberholzer, G.G. Scherer, E.H. Lehmann, Trans. JSME (B) 76 (2010) 1964–1972.
[34] Y. Utaka, Y. Tasaki, N. Waki, D. Iwasaki, N. Kubo, K. Shinohara, P. Boillat, P. Oberholzer, G.G. Scherer, E.H. Lehmann, Trans. JSME (B) 76 (2010) 1995–2001.
[35] Y. Utaka, I. Hirose, Y. Tasaki, Int. J. Hydrogen Energy 36 (2011) 9128–9138.
[36] Y. Utaka, Y. Tasaki, C. Miyata, D. Iwasaki, S. Kondo, O. Aoki, Trans. JSME (B) 76 (2010) 1586–1593.
[37] R. Koresawa, T. Daitoku, Y. Utaka, K. Uesugi, Trans. JSME (B) 77 (2011) 2019–2027.
[38] R. Koresawa, T. Daitoku, Y. Utaka, Trans. JSME (B) 79 (2013) 1038–1050.
[39] L.C. Clark Jr., R. Wolf, D. Granger, Z. Tayor, J. Appl. Physiol. 6 (1953) 189–193.
[40] S. Goto, K. Takeshita, Y. Suzuki, H. Ohashi, Y. Asano, H. Kimura, T. Matsushita, N. Yagi, M. Isshiki, H. Yamazaki, Y. Yoneda, K. Umetani, T. Ishikawa, Nucl. Instrum. Methods Phys. Res. Sect. A 467-468 (2001) 682–685.